ELSEVIER

Deep-Sea Research II 52 (2005) 1671–1683

DEEP-SEA RESEARCH
PART II

www.elsevier.com/locate/dsr2

Response of the southwestern Japan/East Sea to atmospheric pressure

Jae-Hun Park, D. Randolph Watts*

Graduate School of Oceanography, University of Rhode Island, 215 South Ferry Road, Narragansett, RI 02882-1197, USA

Received 18 July 2002; received in revised form 5 August 2003; accepted 11 August 2003
Available online 21 July 2005

Abstract

The response of the southwestern Japan/East Sea (JES) to atmospheric pressure (P_{atm}) and wind-stress ($\vec{\tau}$) forcing is investigated by analyzing 2-year bottom pressure (P_{bot}) data and coastal tide-gauge records. Coherence analyses between P_{bot} data reveal that the response of the southwestern JES is nearly uniform at frequencies lower than 0.6 cycles per day (cpd). The Ulleung Basin (UB) average P_{bot} ($\overline{P}_{bot}$) departs significantly from inverted-barometer (IB) response to the basin average P_{atm} ($\overline{P}_{atm}$) at frequency bands from 0.2 to 0.7 cpd. The coherence between $\overline{P}_{atm}$ and $\overline{P}_{bot}$ has maximum value at 0.2 cpd. Multiple coherence analysis, applied with $\overline{P}_{atm}$ and UB average $\vec{\tau}$ ($\overline{\vec{\tau}}$) as inputs and $\overline{P}_{bot}$ as output, reveals that $\overline{P}_{atm}$ is the most significant forcing, with a peak at frequencies between 0.2 and 0.3 cpd. A simple model [Garrett, 1983. Variable sea level and strait flows in the Mediterranean: a theoretical study of the response to meteorological forcing. Oceanologica Acta 6, 79–87; Lyu et al., 2002. Atmospheric pressure-forced subinertial variations in the transport through the Korea Strait. Geophysical Research Letters 29, 10.1029/2001GL014366] is used to investigate the limiting role of the three straits on the JES response to P_{atm}. Coastal sea-level (η) data inside the JES as well as outside the straits demonstrate that the JES responds with a damped Helmholtz-like resonance. The resonance frequency predicted by this simple model is near the frequency of maximum coherence between $\overline{P}_{atm}$ and $\overline{\eta}_d$, estimated from $\overline{P}_{bot}$ by the hydrostatic approximation. Phase relations and response function gain between these variables confirm the applicability of this simple model to the JES for low-frequency bands below the Helmholtz-like resonance frequency. At higher frequencies, the response relaxes back toward IB, which suggests the mass field adjusts internally within the JES.

1. Introduction

The response to atmospheric pressure (P_{atm}) differs between the open ocean and a semi-enclosed sea. The former has nearly an isostatic response called the inverted-barometer (IB) effect (Brown et al., 1975). The latter depends on the

*Corresponding author. Tel.: +1 401 874 6507; fax: +1 401 874 6728.
E-mail address: rwatts@gso.uri.edu (D.R. Watts).

0967-0645/$ - see front matter © 2005 Elsevier Ltd. All rights reserved.
doi:10.1016/j.dsr2.2003.08.007

frequency of P_{atm} because the interior mass adjustment is restricted by the channels that connect the semi-enclosed sea to the open ocean. In general, at sufficiently low-frequency P_{atm} forcing, water has enough time to exchange through the channels and the interior exhibits isostatic response. However, higher than some particular frequency, the sea-level response differs from the IB effect because the rate of mass exchange through the channels is insufficient. Moreover, wind stress ($\vec{\tau}$) can redistribute mass within the basin on a broad range of frequencies.

The Japan/East Sea (JES) is a semi-enclosed sea that has four straits, among which the Korea Strait is the widest and longest (Fig. 1). As the mass exchange through the Tatarsky Strait is negligible, we expect the Korea, Tsugaru, and Soya Straits in combination to govern the response of the JES to P_{atm}.

Several studies have investigated the sea-level (η) response in the JES at seasonal or interannual periods (e.g., Kang and Lee, 1985; Oh et al., 1993; Kim et al., 2002). Kim et al. (2002) showed, using monthly mean η data, that seasonal time-scale changes of adjusted η at Ulleung Island in the JES are closely associated with the seasonal change of steric height. Fewer studies have investigated the high-frequency response of η in the JES. High-frequency variability on periods of several days to several weeks might be associated with atmospheric forcing from P_{atm} or $\vec{\tau}$. Sokolova et al. (1992) investigated atmosphere-induced η variations along the Korean and Russian coasts of the JES with 3-month-long hourly series of η, P_{atm} and $\vec{\tau}$. They showed that P_{atm} produced the largest contribution to the η variance along eastern Korea for all examined frequencies by applying multiple and partial coherence analyses. However, they were unable to reveal the generally dominant response of the JES, because coastal tidal stations tend to be affected by other local driving forces, producing qualitatively different structures of coherence for each station. Oh et al. (1997) investigated the response to P_{atm} of daily mean η along the coasts of the northwestern Pacific Ocean. They found that η exhibited an abrupt decrease in coherence with P_{atm} at periods shorter than 2–4 days. This nonisostatic response occurred only at stations within the JES. They applied Garrett's single-basin, single-strait theory (Garrett, 1983) to explain that this high-frequency nonisostatic response is caused by the limiting role of the Korea Strait. However, high coherence alone between η and P_{atm} does not mean isostatic response unless in addition they are out of phase with corresponding amplitudes. Recently, a thorough study by Lyu et al. (2002) demonstrated 3–5 day transport variations through the Korea Strait by cross-strait cable voltage fluctuations and direct measurements of the current. They also found an abrupt drop of coherence between η and P_{atm} at periods of 3–4 days. They interpreted these as atmospheric pressure-forced variations using a simple single-basin, three-strait model, with which they calculated a Helmholtz-like resonant period of 3.12 days. However, they noted that both $\vec{\tau}$ and P_{atm} affect the strait transport and η. They ignored variations higher than the Helmholtz-like resonant period.

The relation between η, P_{atm} and bottom pressure (P_{bot}) is accurately expressed from the hydrostatic relation, with the mean water density taken to be ρ_0,

$$\eta = (P'_{bot} - P_{atm})/\rho_0 g, \quad (1)$$

where $P'_{bot} = P_{bot} - \rho_0 g H$, g gravitational acceleration, H the depth of water column in a steady state. All subsequent variables P'_{bot} drop the prime in this paper. Hence in the open ocean P_{bot} represents η if P_{atm} is known at the P_{bot} site (we assume changes in ρ_0 are negligible). The advantage of using P_{bot} data is that unlike coastal η data, they are free from localized contaminating effects.

The aim of this study is to investigate the response of the JES to atmospheric forcing using P_{bot} data. Our focus is upon the variation of P_{bot} at time scales ranging from 1 day to several weeks. We will use 2-year-long records of 12 h P_{bot} data in the southwestern JES plus some coastal η data. The response of the JES is investigated by conducting spectral analyses of P_{bot}, P_{atm}, and η. The dominant effect of P_{atm} on the response is demonstrated with a multiple coherence analysis. The results are then compared with a simple model suggested by Lyu et al. (2002), which takes into account the role of three straits of the JES. Lastly,

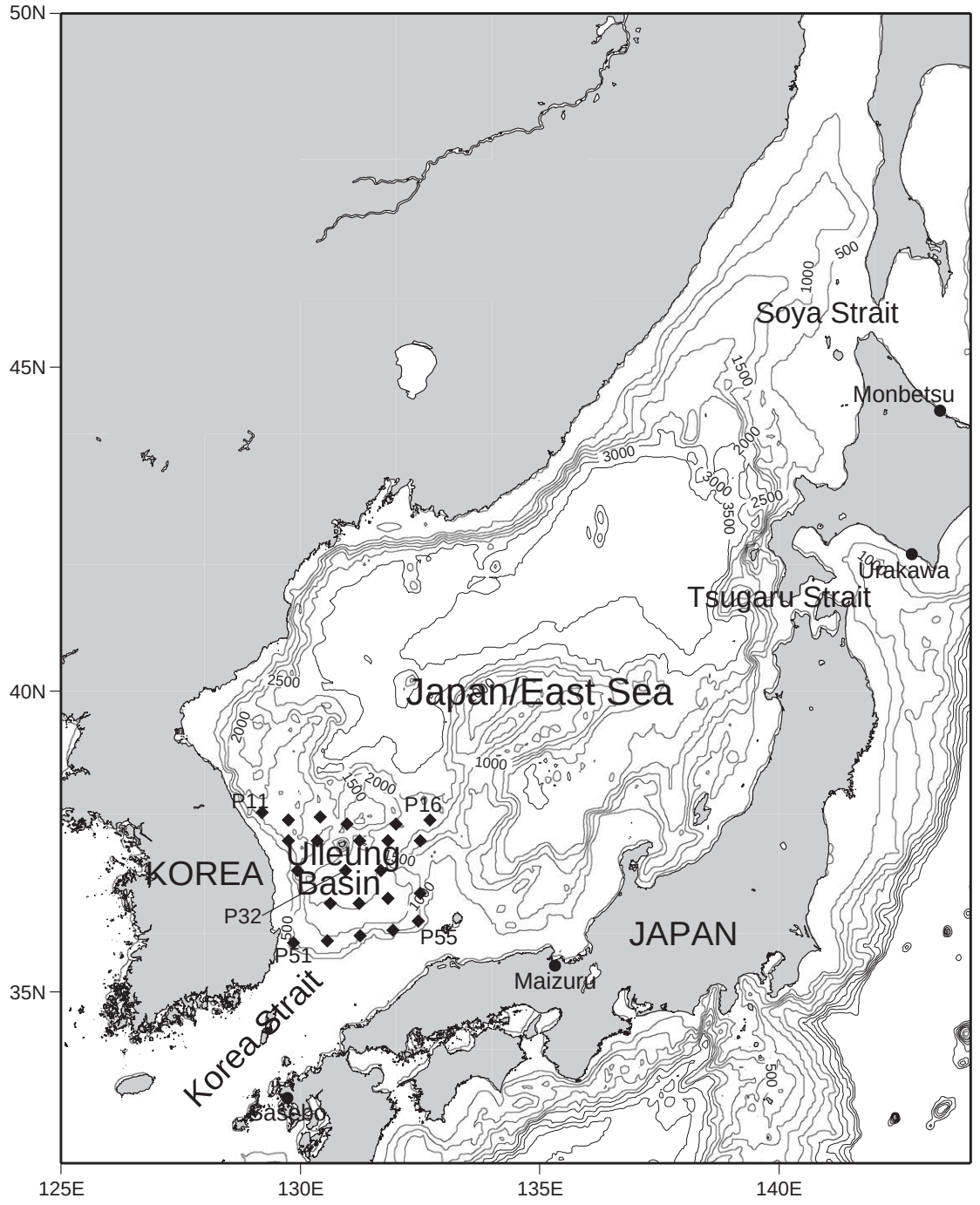

Fig. 1. The Japan/East Sea. Solid diamonds indicate PIESs and solid circles coastal sea level stations used in this study. Bathymetry contours are in meters.

we will show that the dominant response of P_{bot} and η in the JES occurs at a damped Helmholtz-like resonance period of 5 days.

2. Data

During 1999–2001, an array of pressure-sensor-equipped inverted echo sounders (PIESs) was deployed in the southwestern JES for about 2 years (Fig. 1). The array was designed to have 55–60 km spacing between mooring sites and to cover all of the Ulleung Basin (UB). The Paroscientific Digiquartz pressure sensors recorded hourly P_{bot} with better than 1 mm resolution and 0.1–0.3 dbar accuracy. Twenty-three PIESs were recovered successfully and used in this study. Diurnal and semi-diurnal tidal signals were eliminated from all of the P_{bot} records by the response analysis method (Munk and Cartwright, 1966). Details of the moorings are given in the companion paper by Mitchell et al. (2005).

We also use hourly values of η at Maizuru, Sasebo, Urakawa and Monbetsu, Japan, from the same time interval. The data, collected from tide-gauge observations along the Japan coast, were obtained from the Japan Oceanographic Data Center (JODC) website. The Maizuru station is located inside the JES, and the others are just outside of the Korea, Tsugaru and Soya Straits (Fig. 1). The diurnal and semi-diurnal tidal signals also were filtered from these records.

The reanalyzed P_{atm} and $\vec{\tau}$ data come from Navy Operational Global Atmospheric Prediction System (NOGAPS). They are on a degree grid with time interval 12 h.

As our interest is in periods longer than 24 h, the P_{bot} and coastal η data were subsampled every 12 h, corresponding to the atmospheric data. Every data set we used has 1477 values from 00:00GMT, June 16, 1999 to 00:00GMT, June 23, 2001.

Time series of P_{bot}, coastal η at Maizuru and Sasebo and UB average atmospheric pressure ($\overline{P}_{atm}$) are shown in Figs. 2(a), (b) and (c), respectively. $\overline{P}_{atm}$ was calculated by averaging values at nine grid points between 130–132°E and 36–38°N chosen to span the UB. The means have been removed from all of the time series in Fig. 2. Strikingly, all the P_{bot} records showed nearly identical variations through two years, even though the mooring sites span the four corners of the UB with separations as large as 350 km between P11 and P55. Although the coastal η and $\overline{P}_{atm}$ records have noticeable seasonal signals, it is absent from the P_{bot} records. Of course the steric warming that affects η does not change the mass nor P_{bot}. Furthermore we infer from this figure that at seasonal periods, the mass field inside the JES adjusts with an IB response.

High-frequency variations at time scales of several days are shown in all of the time series in Fig. 2. As will be shown by the spectral analyses in next section, these variations of P_{bot} are mainly caused by those of $\overline{P}_{atm}$, but with phase shifts and gains that differ from an isostatic response. An extraordinary maximum of P_{bot} occurred on about the end of October 1999. The coastal η at Maizuru also shows a peak at the same time. This extreme peak is likely to be caused by the maximum volume transport through the Korea Strait in October, 1999, which was reported by Teague et al. (2002).

3. Results

3.1. Spectral analysis of bottom pressure data

All time series had their mean and a linear trend removed prior to spectral analysis. The technique of block averaging in the frequency domain was used to smooth the spectra (Emery and Thomson, 2001). The time series were divided into 50% overlapped equal-length blocks each having 128 data points, and final results ensemble-average the spectra of all blocks. The Nyquist frequency is 1 cycle per day (cpd) and the maximum observable period is 64 days because of the time step (12 h) and length of block, respectively. All spectral analyses in this study use this same procedure.

Variance-preserving power spectra of P_{bot} for three representative sites (P11, P16 and P55) are nearly identical, in accord with the time series of the P_{bot} records (Fig. 3). All show the same peaks at 0.2 cpd. The coherences between pairs of P_{bot}

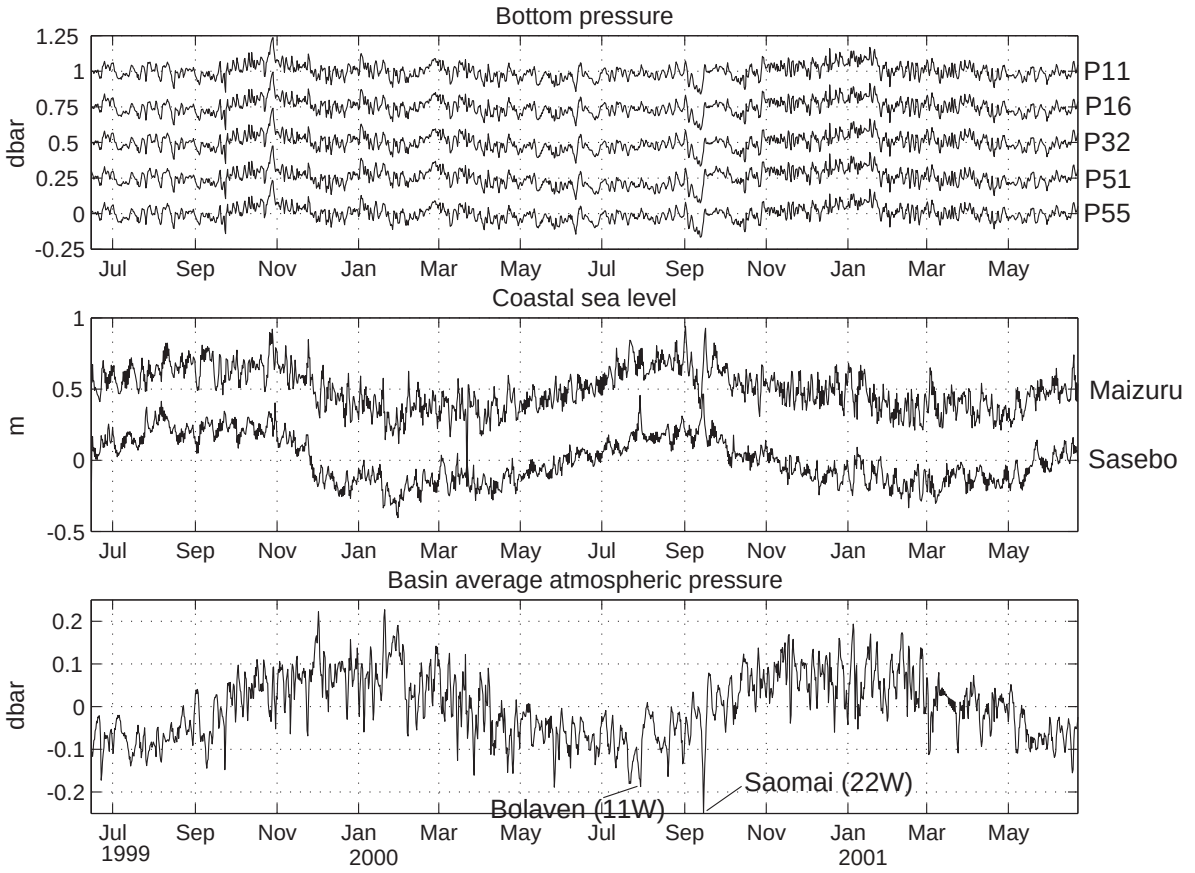

Fig. 2. Time series of bottom pressure (P_{bot}) at P11, P16, P32, P51 and P55 (a), coastal sea level (η) at Maizuru and Sasebo (b), and UB average atmospheric pressure ($\overline{P}_{atm}$) (c), from 00:00GMT, June 16, 1999 to 00:00GMT, June 23, 2001.

data (not shown here) are almost unity from low frequency to 0.6 cpd, while at higher frequencies they drop to approximately 0.8 but remain far above the significance level. The phases (not shown here) remain near 0° through all analyzed frequencies. This indicates that the depicted P_{bot} signal is nearly uniform throughout the UB. This is compatible with the relatively short adjustment time scale set by long gravity waves (barotropic Kelvin waves) travelling in the JES. For example, if we take the length and depth scale of the JES as 1.4×10^6 m and 1350 m, respectively, the time scale of gravity wave propagation is $\sqrt{9.8 \times 1350}/(1.4 \times 10^6) \simeq 3.4$ h. Within just the UB, this time scale is about 1 h. Because of this, in analyzing data at 12-hour intervals we average together our 23 time series of bottom pressure ($\overline{P}_{bot}$) in our following analyses. To aid the reader, we summarize the variables used for this study in Table 1.

3.2. Spectral analysis of Ulleung Basin average atmospheric pressure and bottom pressure

The variance-preserving power spectrum of $\overline{P}_{atm}$ has high values at atmospheric synoptic time scales between 14–3.5 d, or 0.07–0.3 cpd (Fig. 4(a)). Theoretically, if the UB were to respond to $\overline{P}_{atm}$ with an IB effect, there should be no coherence and zero response function gain (m/dbar) between

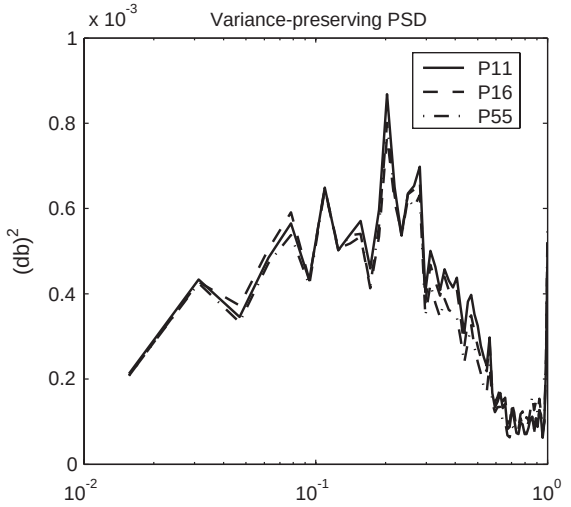

Fig. 3. Variance-preserving power spectra of P11 (solid), P16 (dash) and P55 (dash-dot). The 95% confidence factors are (0.69, 1.60).

Table 1
Definition of variables

Variables	Description
$\overline{P}_{\mathrm{atm}}$	UB average atmospheric pressure
$\overline{P}_{\mathrm{atm0}}$	JES average atmospheric pressure
$\overline{P}_{\mathrm{bot}}$	UB average bottom pressure
$\overline{P}_{\mathrm{bot0}}$	JES average bottom pressure
$\overline{\eta}_{\mathrm{d}}$	UB average sea level obtained from bottom pressure
η_{b}	Sea level in the JES
$\overline{\vec{\tau}}$	UB average wind stress

$\overline{P}_{\mathrm{atm}}$ and $\overline{P}_{\mathrm{bot}}$. This is exhibited for low frequencies below 0.1 cpd (Fig. 4(b), (c)). However, the coherence and gain abruptly increase above 0.5 at 0.2 cpd and remain high until 0.7 cpd. This means that the UB response to $\overline{P}_{\mathrm{atm}}$ differs from

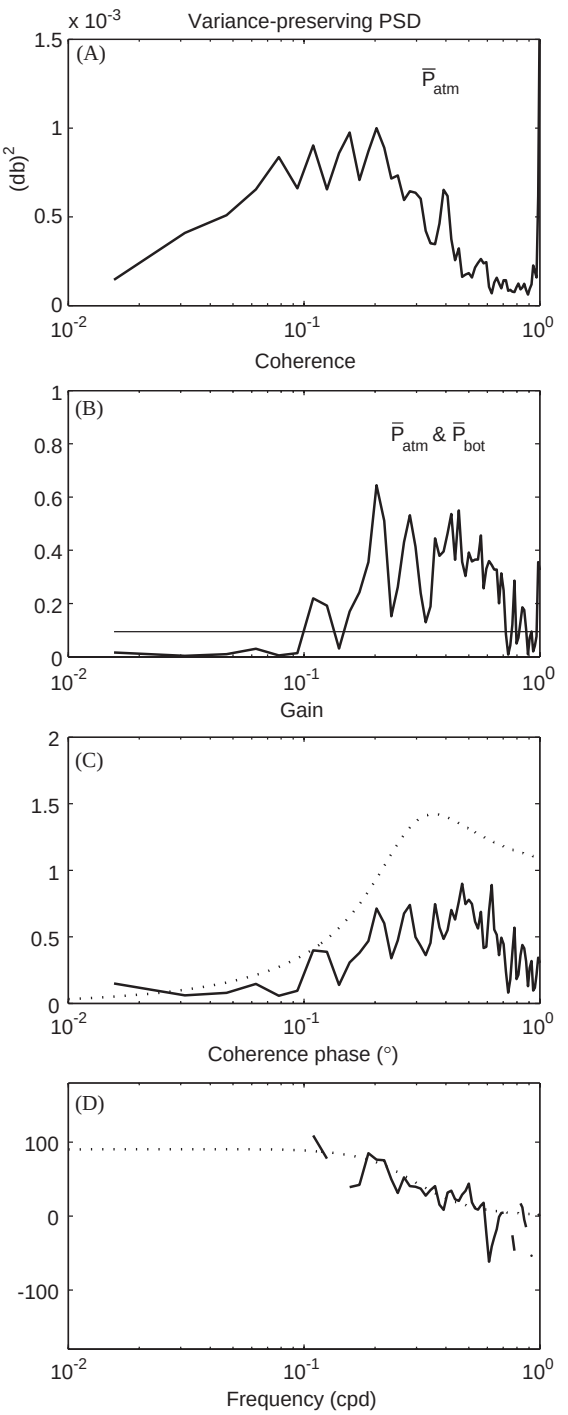

Fig. 4. (a) Variance-preserving power spectra of $\overline{P}_{\mathrm{atm}}$. The 95% confidence factors are (0.69, 1.60). Coherence (b), gain (c) and phase (d) between $\overline{P}_{\mathrm{atm}}$ and $\overline{P}_{\mathrm{bot}}$. The horizontal thin line in (b) indicates the 95% significance level. Phase is omitted if coherence is lower than the significance level. The dotted lines in (c) and (d) represent the theoretically computed gain and phase, respectively. In (d) positive phase represents $\overline{P}_{\mathrm{atm}}$ leading $\overline{P}_{\mathrm{bot}}$.

IB qualitatively between 0.2 and 0.7 cpd. The phase has no meaning when the coherence is low, but within the coherent band it decreases with increasing frequency from about 80° to 0, with $\overline{P}_{atm}$ leading $\overline{P}_{bot}$ (Fig. 4(d)). The phase relation between $\overline{P}_{atm}$ and $\overline{P}_{bot}$ will be interpreted in the next section.

The low coherence (and gain) at yet higher frequencies above 0.7 cpd arises partly because less forcing-variance is present in $\overline{P}_{atm}$, but this also suggests that other processes may be active. The η values inside the JES and outside the connecting straits have insufficient time to equilibrate through water exchange for those high-frequency motions, in contrast to the low frequencies. So it might at first seem surprising for the response to return toward IB at high frequencies. However, internal adjustments within the basin (rather than the entire JES being "compact" with η the same everywhere) could reenable the IB response if the spatial scale of the $\overline{P}_{atm}$ is less than the basin scale. Garrett and Majaess (1984) reported on internal basin adjustments in the Mediterranean Sea at frequencies higher than about 0.5 cpd.

The response of the JES to typhoons might provide examples of these internal basin adjustments. Two typhoons, Bolaven (11 W) and Saomai (22 W), passed through the PIES mooring array during 2000 (2000 Annual Tropical Cyclone Report in website of Naval Pacific Meteorology and Oceanography Center/Joint Typhoon Warning Center). During the two storm passages, η measurements at Maizuru and Sasebo show high peaks (Fig. 2). However, P_{bot} records reveal no distinctive response to the typhoon passages—providing an example in which IB response returns at high frequencies.

3.3. Multiple coherence analysis

In general, mutual coherences between $\overline{P}_{atm}$ and $\vec{\tau}$ are high. Because of this significant coherence, the ordinary single coherence analysis, between P_{bot} (or η) as an output and any one of these atmospheric forcings as a single input, would be physically incorrect. A way to account for mutual correlations between inputs is multiple coherence analysis. Furthermore, using partial coherence analysis, we can separately identify the contribution of each input to the output as a function of frequency (Bendat and Piersol, 2000).

The partial and multiple coherence are estimated between three inputs, $\overline{P}_{atm}$ and x and y components of UB average wind stress ($\overline{\tau}_x$ and $\overline{\tau}_y$), and one output $\overline{P}_{bot}$ (Fig. 5(a)). They reveal that the high coherence obtained by single coherence between 0.2 and 0.7 cpd has some contributions from $\vec{\tau}$. Generally, low-frequency motions are influenced by $\overline{\tau}_y$ and high-frequency motions by $\overline{\tau}_x$. Insignificantly low coherence between $\overline{P}_{atm}$ and $\overline{P}_{bot}$ at the lowest analyzed frequencies, which was shown by the single coherence analyses, is confirmed by the partial coherence. While the $\overline{P}_{atm}$ forcing remains dominant in the 0.2–0.3 cpd frequency band, and the multiple coherence remains high to at least 0.7 cpd, the partial coherences are individually strikingly smaller than obtained from the single coherence analysis. The maximum coherence peak is close to 0.7 at a period of 5 days for both the $\overline{P}_{atm}$ partial coherence and the multiple coherence. The phases between $\overline{P}_{atm}$

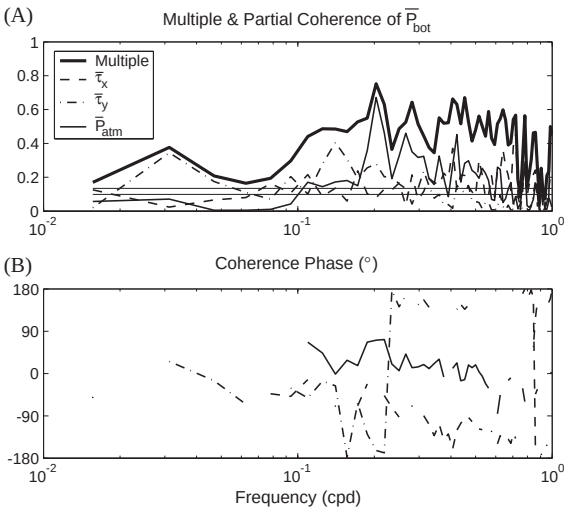

Fig. 5. (a) Multiple and partial coherences between three inputs ($\overline{P}_{atm}$, $\overline{\tau}_x$ and $\overline{\tau}_y$) and one output ($\overline{P}_{bot}$). (b) Phases for the same pairs. Two horizontal thin lines in (a) indicate 95% significance level for multiple (upper line) and partial (lower line) coherences. Phase is omitted if coherence is lower than the significance level.

and $\overline{P}_{bot}$ remain almost the same as those from the single coherence analysis (Fig. 5(b)).

4. Theory and comparisons with observations

We interpret these results in terms of barotropic response of the semi-enclosed JES having three straits. Our analysis is closely guided by studies of Garrett (1983) and Lyu et al. (2002), but we extend the results to examine additional variables. The basin is treated as compact, and the strait(s) constrain the water-volume transport (Q), with the adjustment time to equilibrate pressures between inside and outside the basin restricted primarily by gravity waves, but importantly modified by Coriolis effects and friction.

Garrett (1983) introduced a simple theoretical model of rotationally influenced flow through a strait, connected to a single basin. He considered a strait, having uniform depth H, width W and length L, and a basin of area A (Fig. 6). By using a sea-level difference between η_m the mouth of the strait and η_b inside the basin $\mathrm{Re}[\Delta\eta e^{-i\omega t}] = \mathrm{Re}[(\eta_m - \eta_b)e^{-i\omega t}]$, the average surface current $\mathrm{Re}[ue^{-i\omega t}]$ through the strait is derived as follows:

$$u = gL^{-1}\Delta\eta[-i\omega + (\lambda + 1/2fWL^{-1})]^{-1}, \quad (2)$$

where λ is the linear friction coefficient for the strait and f Coriolis frequency. Note that to let η_b be spatially uniform is valid as discussed in the previous section since long gravity waves require only 3–4 h to traverse a basin such as the JES. The earth's rotation effect fWL^{-1}, called geostrophic control, in Eq. (2) is modified by the factor $\frac{1}{2}$, based on the correction of Wright (1987) applicable to one compact basin connected to a semi-infinite reservoir. An estimate for the friction coefficient is $\lambda = C_D U_0/H$ with a bottom drag coefficient C_D, average speed U_0 and average channel depth H. If $f = 0$ the flow through the strait is dominated by acceleration (ω) and friction (λ). If $\frac{1}{2}fWL^{-1} \gg \omega, \lambda$, the flow is dominated by geostrophic control. For the Korea, Tsugaru and Soya Straits, U_0 is 0.1, 0.7, 0.4 m s^{-1}, respectively, and the estimated $\lambda + \frac{1}{2}fWL^{-1}$ are obtained as $(0.3 + 1.4) \times 10^{-5}$ s^{-1}, $(1.8 + 0.9) \times 10^{-5}$ s^{-1} and $(3.0 + 2.2) \times 10^{-5}$ s^{-1}, respectively, when the values used by Lyu et al. (2002) are applied (Table 2). For the Korea Strait, geostrophic control is about four times as important as friction and about the same magnitude as ω at 5.2 day period. Therefore, the flow through the Korea Strait is geostrophically controlled at frequencies lower than about 5 day periods. On the other hand, Tsugaru and Soya Straits are strongly constrained by bottom friction.

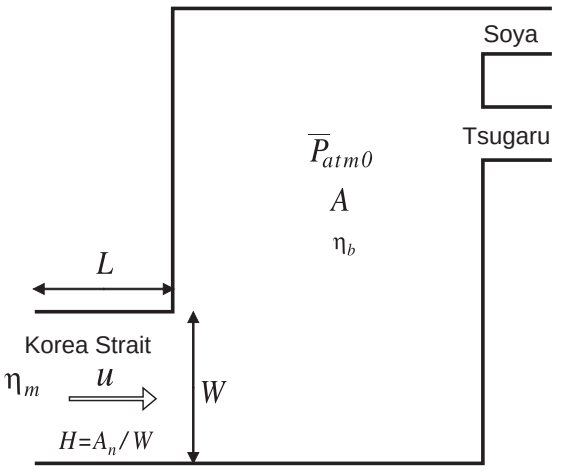

Fig. 6. Schematic of a basin connected to the ocean by three straits. L is the strait length, W the strait width and A the area of basin. Strait flow u is caused by the η difference ($\eta_m - \eta_b$). In the extended model, each strait has its own values for L, W, A_n, u, H and η_m.

Table 2
Summary of the values used for the three channel basin model

Values	Description
$A = 1.3 \times 10^{12}$ m^2	Surface area of the JES
$A_1 = 1.2 \times 10^5 \times 100$ m^2	Cross-sectional area of Korea Strait
$A_2 = 1.9 \times 10^4 \times 120$ m^2	Cross-sectional area of Tsugaru Strait
$A_3 = 4.8 \times 10^4 \times 40$ m^2	Cross-sectional area of Soya Strait
$L_1 = 4.0 \times 10^5$ m	Along-strait length of Korea Strait
$L_2 = 1.0 \times 10^5$ m	Along-strait length of Tsugaru Strait
$L_3 = 1.0 \times 10^5$ m	Along-strait length of Soya Strait
$C_D = 3 \times 10^{-3}$	Bottom drag coefficient
$f = 9 \times 10^{-5}$ s^{-1}	Coriolis frequency
$g = 9.8$ m s^{-2}	Gravitational acceleration
$\rho_0 = 1027$ kg m^{-3}	Mean seawater density

Let $\overline{P}_{atm0}$ denote the average P_{atm} all over the basin, which we treat as the forcing to the basin, and let η'_m be any departure from an IB response at the mouth outside of the strait. Then the following relation between η_b and $\overline{P}_{atm0}$ arises by combining the momentum equations and the mass conservation relation (Garrett, 1983):

$$\eta_b = [\eta'_m - (\rho_0 g)^{-1}\overline{P}_{atm0}]\left[1 - \frac{\omega^2}{\omega_r^2} - i\left(\lambda + \frac{fW}{2L}\right)\frac{\omega}{\omega_r^2}\right]^{-1}. \quad (3)$$

This relation indicates that η_b and $\overline{P}_{atm0}$ are out of phase/in phase at low/high frequencies and have 90° phase difference, with $\overline{P}_{atm0}$ in the lead, at a Helmholtz-like resonance frequency ω_r defined as

$$\omega_r^2 = \frac{gHW}{AL}. \quad (4)$$

When $\omega \ll \omega_r$ and $\eta'_m = 0$, η_b and $\overline{P}_{atm0}$ have an IB response relation.

To extend Garrett's model to a multi-channel model is straightforward. Lyu et al. (2002) used a three-channel model applicable to the JES. The relation between η_b and $\overline{P}_{atm0}$ in the multi-channel model can be obtained as follows if we approximate η'_m as zero (exact IB response in the external reservoirs):

$$\eta_b = \frac{-1}{\rho_0 g(1 - 1/\Sigma)}\overline{P}_{atm0}, \quad (5)$$

where

$$\sum = \sum_n \left\{\frac{\omega^2}{\omega_n^2} + i\left(\lambda_n + \frac{fW_n}{2L_n}\right)\frac{\omega}{\omega_n^2}\right\}^{-1} \quad (6)$$

and ω_n is the Helmholtz-like resonance frequency for the nth channel (see Appendix).

Spectral analyses between the coastal η at Sasebo, Urakawa and Monbetsu stations outside each respective strait and local P_{atm} inform us about the neglected η'_m (Fig. 7). The coastal η record at Maizuru is also analyzed to exhibit the different response of η inside versus outside of the JES.

At Sasebo the variance-preserving power spectrum of η shows a peak at 0.07 cpd (14 d), which is longer than the atmospheric synoptic forcing. Hence, this is likely caused by other physical processes such as Kuroshio variation, since the coherence at this frequency is relatively low (but still far above the significance level). The strongest spectral density near 1 cpd represents tidal signals. The maximum coherence peak close to 0.9 is shown at 0.2 cpd. The gain is close to unity from very low frequency to 0.4 cpd. The phase is steady and close to 180° (Fig. 7(g)).

At Urakawa the variance-preserving power spectrum of η reveals high values at a frequency lower than 0.1 cpd. However, the coherence shows high values between 0.1 and 0.5 cpd. This indicates that the η variations at Urakawa longer than 10-day period arise mainly from another physical process. However, within the band 0.1–0.7 cpd, of main interest to the response of the JES, the observed high coherence, unity gain, and 180° phase correspond to IB response, as was assumed for the above model.

The coherence of η at Monbetsu with local P_{atm} shows low values at most frequencies, indicating influence by other processes, either non-IB response within the Okhotsk or because Monbetsu is on the left side of the channel looking in, which differs from Garrett's assumption of Kelvin wave adjusted height. (We have no access yet to Russian tide station data on the right side, which is Kamchatka Peninsula.) Nevertheless the gain and phase at Monbetsu reveal IB response-like relations from very low frequency to 0.5 cpd.

Overall, these results indicate that the outside regions of the three straits connecting the JES to the East China Sea and northwestern Pacific Ocean exhibit some differences from IB response to P_{atm}. Neglecting η'_m in Eq. (3) might cause some errors in the theoretical interpretation, but this would be a subject for future study requiring a more complete atmosphere–ocean coupled model.

At Maizuru the variance-preserving power spectrum of η exhibits a peak at 0.2 cpd (Fig. 7(a)). The gain and phase results differ from those outside the straits. The gain peaks are at 0.2 and 0.4 cpd, and the phase decreases from 180° to 20° at frequencies lower than 0.5 cpd. These results agree well with those of Lyu et al. (2002). The gain peak at 0.4 cpd is likely indirectly affected by $\vec{\tau}$,

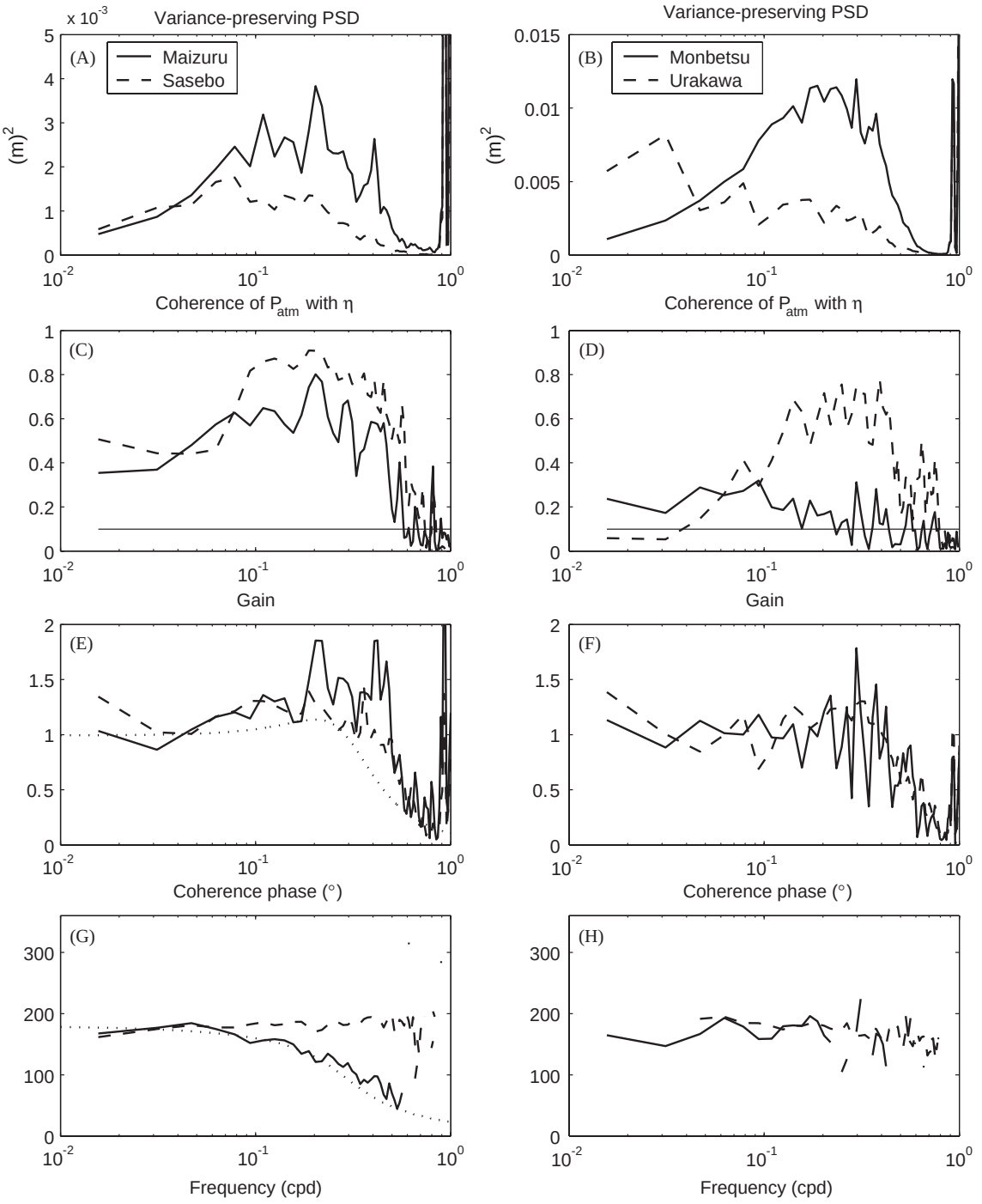

Fig. 7. Variance-preserving power spectra of coastal η at (a) Maizuru, Sasebo, (b) Urakawa and Monbetsu. The 95% confidence factors are (0.69, 1.60). (c, d) Coherence, (e, f) gain and (g, h) phase between local P_{atm} and η at each of the four coastal locations. The horizontal thin line in (c) and (d) indicates the 95% significance level. Phase is omitted if coherence is lower than the significance level. The dotted lines in (e) and (g) represent the theoretically computed gain and phase, respectively.

analogous to our results displayed in Fig. 5 for $\overline{P}_{\mathrm{bot}}$.

To compare the simple model expressed by Eq. (5) to our observational data inside the JES, we also conducted multiple coherence analysis between atmospheric forcings and $\overline{\eta}_{\mathrm{d}}$. We approximate $\overline{\eta}_{\mathrm{d}} = (\rho_0 g)^{-1}(\overline{P}_{\mathrm{bot}} - \overline{P}_{\mathrm{atm}})$ from Eq. (1). The atmospheric forcing variables are $\overline{P}_{\mathrm{atm0}}$, $\overline{\tau}_x$ and $\overline{\tau}_y$, where $\overline{P}_{\mathrm{atm0}}$ is estimated by averaging P_{atm} spatially over the JES. The multiple and partial coherence results in Fig. 8 reveal that P_{atm} is the dominant forcing for η as well as for P_{bot}. Reminiscent of Fig. 5, the maximum partial coherence between $\overline{P}_{\mathrm{atm0}}$ and $\overline{\eta}_{\mathrm{d}}$ is also shown at 0.2 cpd. The phase is observed to follow strikingly well the theoretically calculated decrease from 180° to 100° at frequencies lower than 0.3 cpd, using the values in Table 2. This decreasing trend is also similar to the result of Lyu et al. (2002), which they obtained by averaging coastal η inside the JES. However, the phase increases again (returning to 180° IB response) at frequencies higher than 0.5 cpd. This increasing trend of phase for frequencies higher than 0.33 cpd, becoming out of phase again around 0.7 cpd, might be caused by internal (IB) adjustments as explained in the previous section.

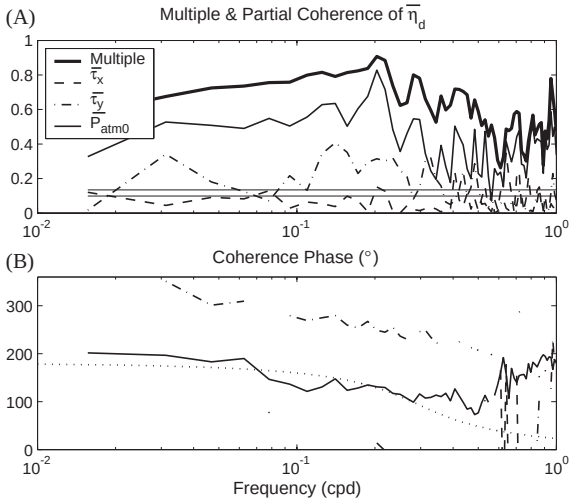

Fig. 8. (a) Multiple and partial coherences between three inputs ($\overline{P}_{\mathrm{atm0}}$, $\overline{\tau}_x$ and $\overline{\tau}_y$) and one output ($\overline{\eta}_{\mathrm{d}}$). (b) Phases for the same pairs. Two horizontal thin lines in (a) indicate 95% significance level for multiple (upper line) and partial (lower line) coherences. Phase is omitted if coherence is lower than the confidence level. The dotted line in (b) represents the theoretically computed phase.

The partial coherences between $\overline{\vec{\tau}}$ and $\overline{\eta}_{\mathrm{d}}$ show that the contributions of $\overline{\tau}_y$ are significant at frequencies lower than 0.4 cpd. The decreasing trend of phase from in-phase to out-of-phase between $\overline{\tau}_y$ and $\overline{\eta}_{\mathrm{d}}$ demonstrates the response of the JES to the $\overline{\tau}_y$ forcing. At very low frequencies, the water mass forced by $\overline{\tau}_y$ blowing southward, for example, has enough time to exit the JES through the Korea Strait. Otherwise, at high frequencies, it accumulates in the southern JES, which makes the response out-of-phase.

A relation between $\overline{P}_{\mathrm{atm0}}$ and average P_{bot} over the JES ($\overline{P}_{\mathrm{bot0}}$) may be obtained by substituting $\mathrm{Re}[\eta_{\mathrm{b}} e^{-i\omega t}] = (\rho_0 g)^{-1}\ \mathrm{Re}[(\overline{P}_{\mathrm{bot0}} - \overline{P}_{\mathrm{atm0}})e^{-i\omega t}]$ into Eq. (5)

$$\overline{P}_{\mathrm{bot0}} = \frac{1}{1-\Sigma}\,\overline{P}_{\mathrm{atm0}}. \tag{7}$$

The computed gain and phase between $\overline{P}_{\mathrm{atm0}}$ and $\overline{P}_{\mathrm{bot0}}$ are shown as dotted lines in Fig. 4(c) and (d), respectively. Our bottom pressure observations cover only the southwestern JES, so we have available only an approximation to $\overline{P}_{\mathrm{bot0}}$ for estimating $\overline{P}_{\mathrm{bot}}$. However, the computed gain and phase relations for $\overline{P}_{\mathrm{bot0}}$ are consistent with the observed values between 0.1 and 0.5 cpd (Fig. 4) where coherence is above the significance level, except that the observed $\overline{P}_{\mathrm{bot}}$ gain peak is less pronounced than the theoretically predicted.

Without frictional and geostrophic constraints, $\lambda + \frac{1}{2}fWL^{-1}$, in the channels, both Eqs. (5) and (7) would reveal the same Helmholtz-like resonance frequency of 0.32 cpd using the channel sizes in Table 2. However, due to these constraints, the two damped Helmholtz-like resonance frequencies (i.e. gain maxima) are at 0.2 and 0.35 cpd for η and P_{bot}, respectively (Figs. 7(e) and 4(c)). This prediction is inconsistent with the observed P_{bot} coherence curve, which shows the same resonance frequency of 0.2 cpd (Fig. 5(a)) as for η (Fig. 8(a)). This discrepancy might be caused by inadequate assumptions for the simple model, such as neglecting η'_{m} and assuming compactness (uniform η all over the JES). The corresponding reduction

of the high-frequency response would shift the observed P_{bot} peak to a lower frequency.

5. Summary

The response of the southwestern JES to P_{atm} shows a significant departure from the IB response at frequencies between 0.2 and 0.7 cpd, at which the coherences between $\overline{P}_{atm}$ and $\overline{P}_{bot}$ show high values. At low (<0.2 cpd) and high frequencies (>0.7 cpd), IB responses are observed. Multiple and partial coherence analyses enable us to distinguish the contributions of the atmospheric forcings. They show that $\overline{P}_{bot}$ variations around 0.2–0.3 cpd are predominantly induced by $\overline{P}_{atm}$, with maximum coherence at 0.2 cpd. The coherence curves are close to the theoretically computed damped Helmholtz-like behavior predicted by a simple model. The phase relations between $\overline{P}_{atm}$ and $\overline{P}_{bot}$ also agree well with those predicted from the model.

The $\overline{\eta}_d$, estimated hydrostatically in mid-basin, shows respectively decreasing and increasing trends in the phase relation with $\overline{P}_{atm0}$ at low (<0.3 cpd) and high (>0.5 cpd) frequencies. The decreasing trend is consistent with a theoretically calculated phase relation from the simple model. We suggest the increasing trend is caused by internal adjustments, which are not taken into account in the simple model. The additional response of the JES to wind stress is exemplified by the phase relation of $\overline{\eta}_d$ with $\overline{\tau}_y$. At low frequencies, water-mass exchange through the Korea Strait induced by $\overline{\tau}_y$ forcing is enough to change η inside the JES; whereas at high frequencies the water mass accumulates or depletes in the southern JES, and hence raises or lowers η.

This study demonstrates that the JES responds to atmospheric pressure as an IB effect at the lowest (<0.2 cpd) frequencies. The Korea, Tsugaru and Soya Straits modify this IB response of the JES to the atmospheric forcing. At mid-frequencies (0.2–0.7 cpd), the JES has a damped Helmholtz-like resonance response that departs substantially from the IB response. As this band also contains the greatest variance in P_{atm}, the SSH (η) inside the JES departs significantly from IB—a fact to bear in mind when interpreting satellite altimeter observations there. At frequencies higher than 0.7 cpd, P_{atm} spatial scales are smaller and internal adjustments restore the response back toward an IB response. The simple three-channel model has clearly identified the processes, and a numerical model would be required to achieve substantially improved prediction of the response of the JES to atmospheric forcing. The roles of the neighboring Yellow Sea, East China Sea, the northeastern Pacific Ocean, and Okhotsk Sea should probably be included in such a model.

Acknowledgments

We thank Douglas Mitchell and Karen Tracey for their help in processing the bottom pressure data. Thanks also to Mark Wimbush and Sang Jin Lyu for their useful comments and advice on this work. William J. Teague kindly provided us NOGAPS atmospheric data. Comments from anonymous reviewers were helpful for the improvement of this paper. This work was supported by the Office of Naval Research "Japan/East Sea DRI". Basic Research Programs include the Japan/East Sea initiative under Grant N000149810246 and the Naval Research Laboratory's "Linkages of Asian Marginal Seas" under Program Element 0601153N.

Appendix A

To extend Garrett's model to a multi-channel model, having a single compact basin and n channels to separate reservoirs, the governing equations are mass conservation and momentum balance, as follows:

$$A\frac{\partial \eta_b}{\partial t} = \sum_n Q_n, \tag{A1}$$

$$\frac{\partial Q_n}{\partial t} = -A_n\frac{\overline{P}_{atm0} + \rho_0 g(\eta_b - \eta'_{m_n})}{\rho_0 L_n} - \left(\lambda_n + \frac{fW_n}{2L_n}\right)Q_n, \quad n = 1, 2, 3, \ldots \tag{A2}$$

where Q_n is the volume transport through the nth channel, $A_n = W_n H_n$ the cross-sectional area of the nth channel, λ_n the linear friction coefficient for the nth channel, and L_n the length of the nth channel. We set η'_{m_n} equal to zero on the assumption that the response at the outside of the channels to P_{atm} is the IB response. If we let η_b, Q_n and $\overline{P}_{atm0}$ be $\mathrm{Re}[\eta_b e^{-i\omega t}]$, $\mathrm{Re}[Q_n e^{-i\omega t}]$ and $\mathrm{Re}[\overline{P}_{atm0} e^{-i\omega t}]$, we obtain Eq. (5). The Helmholtz-like resonance frequency for the nth channel is

$$\omega_n = \frac{gH_n W_n}{AL_n}. \tag{A3}$$

References

Bendat, J.S., Piersol, A.G., 2000. Random Data: Analysis and Measurement Procedures, third ed. Wiley, New York, 594 pp.

Brown, W., Munk, W., Snodgrass, F., Mofjeld, H., Zetler, B., 1975. Mode bottom experiment. Journal of Physical Oceanography 5, 75–85.

Emery, W.J., Thomson, R.E., 2001. Data Analysis Methods in Physical Oceanography, second ed. Elsevier, Amsterdam, 638 pp.

Garrett, C., 1983. Variable sea level and strait flows in the Mediterranean: a theoretical study of the response to meteorological forcing. Oceanologica Acta 6, 79–87.

Garrett, C., Majaess, F., 1984. Nonisostatic response of sea level to atmospheric pressure in the Eastern Mediterranean. Journal of Physical Oceanography 14, 656–665.

Kang, Y.Q., Lee, B.D., 1985. On the annual variation of mean sea level along the coast of Korea. Journal of the Oceanology Society of Korea 20, 22–30.

Kim, K., Cho, Y.-K., Choi, B.-J., Kim, Y.-G., Beardsley, R.C., 2002. Sea level variability at Ulleung Island in the East (Japan) Sea. Journal of Geophysical Research 107 (C3).

Lyu, S.J., Kim, K., Perkins, H.T., 2002. Atmospheric pressure-forced subinertial variations in the transport through the Korea Strait. Geophysical Research Letters 29.

Mitchell, D.A., Watts, D.R., Wimbush, M., Teague, W.J., Tracey, K.L., Book, J.W., Chang, K.-I., Suk, M.-S., Yoon, J.-H., 2005. Upper circulation patterns in the Ulleung Basin. Deep-Sea Research II, this issue [doi:10.1016/j.dsr2.2003.09.005].

Munk, W.H., Cartwright, D.E., 1966. Tidal spectroscopy and prediction. Philosophical transactions of the Royal Society of London 259A, 533–581.

Oh, I.S., Rabinovich, A.B., Park, M.S., Mansurov, R.N., 1993. Seasonal sea level oscillation in the East Sea. Journal of the Oceanology Society of Korea 28, 1–16.

Oh, I.S., Moon, I.-J., Youn, Y.-H., 1997. Daily mean sea level and atmospheric pressure along the coasts of the north-western Pacific Ocean. The Journal of the Korean Society of Oceanography 32, 171–180.

Sokolova, S.E., Rabinovich, A.B., Chu, K.S., 1992. On the atmosphere-induced sea level variations along the western coast of the Sea of Japan. La mer 30, 191–212.

Teague, W.J., Jacobs, G.A., Perkins, H.T., Book, J.W., Chang, K.-I., Suk, M.-S., 2002. Low-frequency current observations in the Korea/Tsushima Strait. Journal of Physical Oceanography 32, 1621–1641.

Wright, D.G., 1987. Comments on Geostrophic control of fluctuating barotropic flow through straits. Journal of Physical Oceanography 17, 2375–2377.